Chapter 4. Semiconductor Surface Studies

Academic and Research Staff

Professor John D. Joannopoulos, Dr. Tomas A. Arias, Dr. Robert D. Meade

Graduate Students

Rodrigo B. Capaz, Kyeongjae Cho, Jing Wang

Technical and Support Staff

Imadiel Ariel

4.1 Introduction

Sponsors

Joint Services Electronics Program
Contract DAAL03-92-C-0001

Understanding the properties of the surfaces of solids and the interactions of atoms and molecules with surfaces has been of extreme importance both from a technological and an academic point of view. The advent of ultrahigh vacuum technology has made microscopic studies of well-characterized surface systems possible. The way atoms move to reduce the energy of the surface, the number of layers of atoms involved in this reduction, the electronic and vibrational states that result from this movement, and the final symmetry of the surface layer are all of utmost importance in arriving at a fundamental and microscopic understanding of the nature of clean surfaces, chemisorption processes, and the initial stages of interface formation.

The theoretical problems associated with these systems are quite complex. However, we are currently at the forefront of solving the properties of real surface systems. In particular, we are continuing our efforts to develop new techniques for calculating the total ground-state energy of a surface system from "first principles," so that we can provide accurate theoretical predictions of surface geometries and behavior. Our efforts in this program have concentrated in the areas of surface growth, surface reconstruction geometries, structural phase transitions, and chemisorption.

4.2 Defects on Surfaces

Real surfaces typically contain a variety of imperfections that can be important in determining their electronic and chemical behavior. A particularly interesting system is the vicinal Si(100) surface. The Si(100) surface has been an object of intensive study for the last three decades in part because it is technologically important in semiconductor industry, and in part because its reconstructions are simple enough to be tractable to theoretical investigations.

Although much is understood about the electronic and structural properties of Si(100), there has been relatively little work done to study the nature of intrinsic defects on this surface. Interestingly, scanning-tunneling-microscopy (STM) images of this surface consistently show the presence of a large number of what appear to be missing dimers or dimer vacancies (DV). In fact, a typical STM image of this surface exhibits three striking features. The first is the very large number of missing dimers present on the surface. The second is that the missing dimer defects tend to congregate into small clusters, and the third is that the clusters appear to form distinctive complexes that dominate over others. These results are summarized for a typical image (which had about 22,000 dimer sites in total) in figure 1. The data shown here are from a surface annealed at 700°C and "flashed" up to 1100°C for several minutes. The STM image, however, is taken at room temperature after the sample has cooled down. The STM image therefore represents a quasi-equilibrium "snap-shot" at some freezing-in temperature below 700°C.

In order to unravel this striking behavior, we combined *ab-initio* total energy calculations of the energetics of over 20 defect complexes with statistical mechanical and kinetic arguments to construct a meaningful and realistic theory of this system. Examples of some of the defects and defect complexes studied are shown in figures 2-4. In figure 5

	Pattern	number of defects: N	fraction: n (10^{-3})
1-DV		148	6.7
2-DV		78	3.5
1+2-DV		244	1.1
1+2+1-DV		6	0.3
3-DV		23	1.0
1+3-DV		54	2.5
1+3+1-DV		100	4.5
4-DV		0	0.0

Figure 1. The total number and fraction of various DV, DV clusters, and DV cluster complexes on the surface.

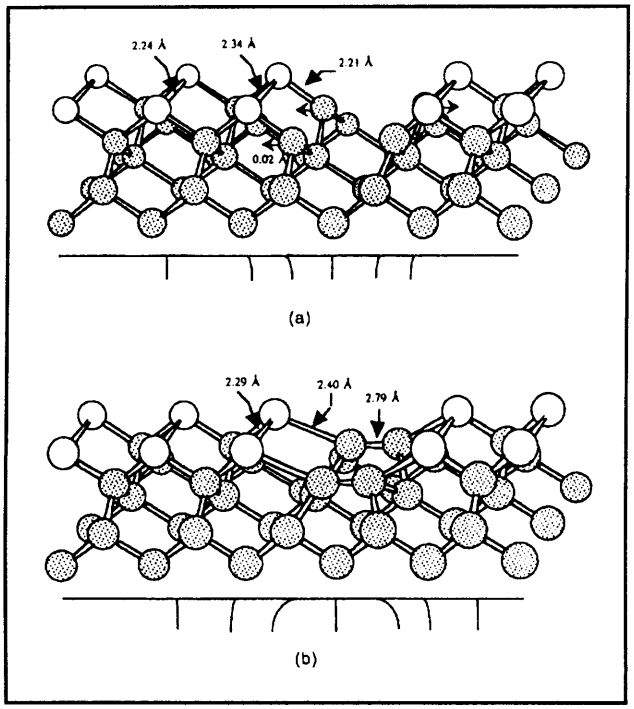

Figure 2. Total energy and restoring force as a surface dimer penetrates the bulk to attempt to form an interstitial dimer. (a) Schematic diagram illustrating three stages of the penetration process. Open circles represent the surface atoms and shaded circles, bulk atoms. (b) The force and formation energy of the dimer as a function of penetration depth. Note the absence of a metastable interstitial-dimer configuration.

we summarize the results of our total energy calculations for some of the most important defects and defect complexes.

Let us now address the problem of predicting the distribution of DV clusters and complexes on the Si

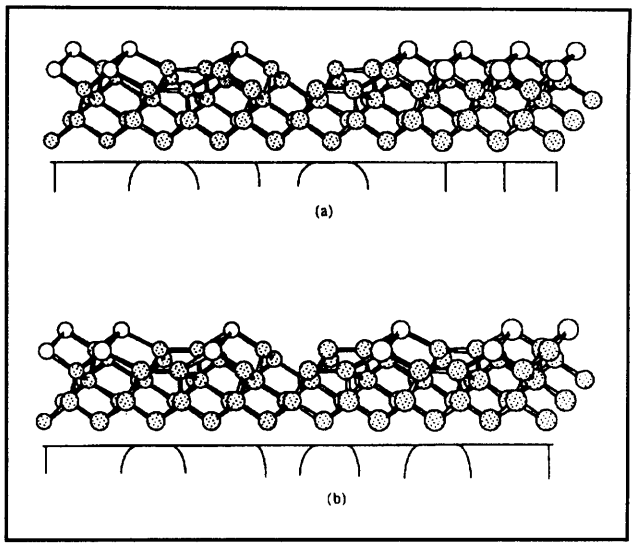

Figure 3. Two stable configurations of the 2-DV based cluster complexes. (a) The stable configuration for (1+2)-DV: the unrebonded side of the 2-DV cluster links with a rebonded 1-DV. (b) The stable configuration of the (1+2+1)-DV: two rebonded 1-DVs link to either side of the 2-DV cluster. The symbols are the same as in figure 2.

surface. The first phase in the analysis of the defect distribution is to determine whether the kinetics of the anneal at 800-1100°C are sufficient to establish a thermal distribution among the defects or whether some trace remains of the initial distribution form cleavage. The kinetic pathways which contribute to the distribution after the initial anneal must have barriers sufficiently low that they may be expected to be traversed during the time scale of the anneal. Taking the waiting time for a transition event to be on the order of 1 minute, the attempt rate to be near the Si optic phonon frequency (the final answer is not sensitive to these values as we eventually take a logarithm), and the probability of a successful traversal to be the Boltzmann factor, we conclude the maximum barrier height for allowed paths in this experiment is 4.0 eV at the peak anneal temperature.

In figure 6, we show the pathways whose energy barriers we find to be near or less than the 4.0-eV cutoff. Note the defects we have considered in this work form a *connected* Markov chain which is tied to the sink and the source of DVs by diffusion of single DVs to the step edges. Therefore, the annealing process will be sufficient to remove all traces of the DV distribution of DV clusters and complexes.

After the initial anneal is completed, the sample is then cooled to room temperature before being scrutinized by the STM. Understanding the behavior of the distribution during this process requires a more detailed look at the transitions between the DV

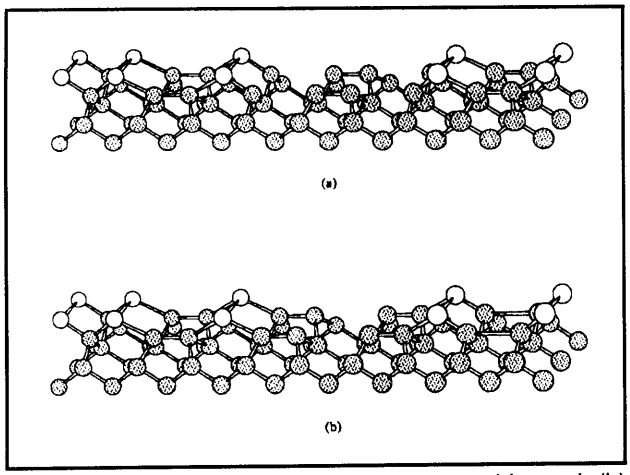

Figure 4. (a) The nearly degenerate stable and (b) metastable configurations of the (1+3+1)-DV cluster complexes. The symbols are the same as in figure 2.

defects. Three broad groups make up these transitions. The first group, indicated by the solid lines in figure 6, have relatively low energy barriers. These transitions all involve processes whereby an isolated dimer vacancy can migrate to an adjacent site. Using our estimates of the three basic types of second-layer rebonds, we find that all the transitons in this class traverse barriers of about 2.5 eV.

The second class of transition, indicated by the dashed lines in figure 6, have significantly higher barriers because they can occur only by disturbing the strong second-layer rebonding adjacent to the moving dimer. The barrier heights for these transitions are more difficult to estimate quantitatively, but our bond counting puts them in the range of 3.5-4.0 eV. The broken solid line in figure 6 represents an example of a third class of transition which we believe to be rare despite its energy barrier being in the first class. This is the transition by which the DV on the far right of the (1+2+1)-DV complex stretched in figure 5 migrates to the left, leaving behind a (1+2)-DV complex. This motion alone results in a high-energy metastable (1+2)-DV complex which can decay into the stable (1+2)-DV complex only by the independent migration of *both* second-layer rebonds across the 2-DV cluster. This particular transition therefore requires three independent motions to occur in concert (the initial dimer migration plus the migration of the rebonds), and so we suggest in our model that the attempt frequency for this transition may be so much reduced from the optic phonon frequency that this pathway is not relevant in the system.

We are now ready to understand the system's behavior as it cools from the anneal. As the system cools, the higher-energy transitions rapidly become inaccessible to the system, severing the

	Configuration	*Ab initio* Calculation	Keating Correction	Formation Energy	Energy Per DV
1-DV		0.35	-0.12	0.22	0.22
2-DV		0.40	-0.07	0.33	0.16
3-DV		0.70	-0.25	0.45	0.15
1+2-DV		0.65	-0.23	0.42	0.14
1+2+1-DV		1.25	-0.38	0.87	0.22
1+3-DV(a)		1.19	-0.38	0.81	0.20
1+3-DV(b)		1.16	-0.39	0.77	0.19
1+3+1-DV(a)		1.30	-0.57	0.73	0.146
1+3+1-DV(b)		1.35	-0.58	0.77	0.154

Figure 5. The formation energy (in eV) of DV, DV clusters, and DV cluster complexes. The second column illustrates the second-layer rebonding. The third column is the formation energy from the *ab initio* calculation, the fourth column the Keating correction, and the fifth and sixth columns are corrected formation energy per structure or per dimer, respectively.

Markov chain into two disconnected parts by removing the dashed pathways shown in figure 6. As a consequence, the system of complexes comprising the upper part of the chain in the figure loses thermal contact with the rest of the system as the temperature drops below 900-1100°C (corresponding to 3.5-4.0 eV). Although low barrier transitions among these complexes continue to occur down to about 570°C (the freeze-in temperature for the lower barrier transitions by the familiar kinetic argument), they cannot change the *total number* of these complexes, which will remain fixed as the system cools. These transitions, however, will affect the *relative* distribution among those complexes, which will track the surface temperature down to the lower freeze-in temperature.

The lower part of the chain, however, remains in contact with the DV source and the sink at the step edges through lower-energy single DV migrations and thus remains in overall thermal equilibrium with the surface until the *lower* freeze-in temperature.

In figure 7 we confirm the predictions of our theory with a plot of our calculated defect energies, E_i, against $-\ln(n_i/g_i)$, where n_i is the experimentally observed defect density. We choose this scaling so that Boltzmann distributed data appear as straight

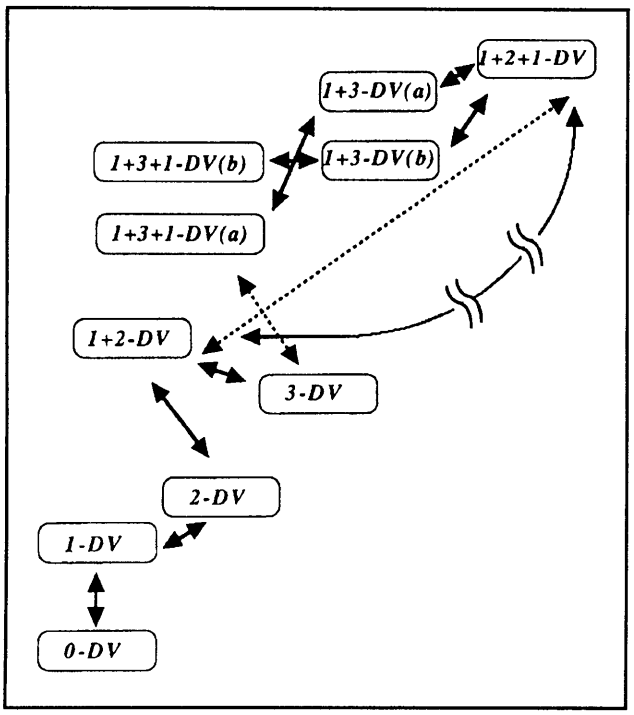

Figure 6. Illustration of the Markov chain formed by the principal DV defects and the primary pathways among them. Dashed lines represent transitions with relatively large energy barriers (~3.5-4.0 eV) which cease to be relevant around 900-1100°C, while solid lines represent transitions of lower energy near 2.5 eV, which essentially shut off around 570°C. The transition with the broken solid line also has a barrier near 2.5 eV, but it is expected to be forbidden by a low attempt frequency.

lines. Our model predicts all of the salient features of this plot. First, the data from the experiment are clearly clustered in two-groupings corresponding exactly to the severed halves of the Markov chain. Second, the lower group, containing the defects which remain in thermal contact with the steps, falls nicely along the predicted 570°C Boltzmann distribution. The (1+2)-Dv complex appears to fall somewhat above the rest of this grouping, probably as a result of the favorable elastic interaction between the stress field of the constituent 1- and 2-DV clusters, which raises the barrier to decay by roughly 0.2 eV, corresponding to a 60°C increase in the freeze-in temperature. Next, the center of the second grouping lies, as expected, within the 900-1100°C Boltzmann distributions, but the grouping exhibits a relative temperature, or slope, observably less than 900°C and more in line with that of the lower freeze-in temperature of 570°C. This final feature is the direct result of the maintenance of local thermal equilibrium among these defects after they have lost thermal contact with the rest of the system.

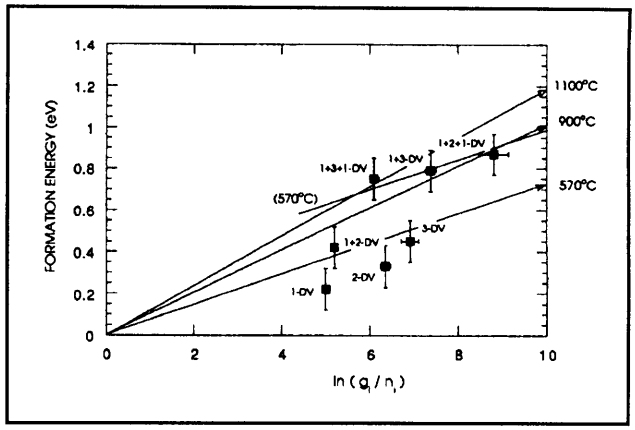

Figure 7. Plot of the *ab initio* formation energy of each defect vs. the logarithm of the *experimental* defect density, n_i, normalized by appropriate degeneracy factors, g_i. Data with absolute Boltzmann distribution at 570, 900, and 1100° C fall along the straight lines indicated in the figure which pass through the origin. A relative Boltzmann distribution (see text for definition and discussion) at 570°C is sketched through the data clustered at the top of the figure. Note that the two groupings of data correspond exactly to the severed parts of the Markov chain in figure 6.

4.3 Cross-sectional Scanning Tunneling Microscopy

Cross-sectional Scanning Tunneling Microscopy (X-STM) is a potentially powerful experimental tool for investigating interface structure in heteroepitaxial growth. An unfortunate problem with STM, however, has been the unambiguous identification of chemical species when several types of atoms are present in a variety of bonding configurations. For example, there are two serious questions which arise when considering an experiment using X-STM to investigate the initial stages of growth in an actual heteroepitaxial system such as GaAs on Si. First, it is not obvious that the isolated Ga and As atoms on the surface of a Si substrate could be uniquely identified, either by the contrast they produced in an X-STM image (induced by charge-density fluctuations) or by changes in the I-V signature of the tunneling current in the vicinity of such atoms. Second, the interactions between the charge-density fluctuations from the cleaved surface of the bulk and the growth Si-doped surface and their impact on the resultant X-STM image are not well-understood. For these two reasons, we have chosen to take a simplified approach as a first step in our investigation of the initial stages of heteorpitaxy of GaAs on Si. We have chosen first to examine, by theoretical methods, the chemical interactions taking place in the vicinity of a plane of impurity atoms embedded in a host crystal, and to predict whether or not unambiguous chemical identification can be performed on an isolated impurity

atom in such a system. By choosing this prototypical "embedded-surface" approach, we can eliminate the additional complications provided by the growth surface. Because we are interested in the atomic interactions between Ga, As and Si, for this work we have chosen to examine the use of Si atoms to dope a GaAs crystal. Doping of semiconducting materials, in which dopant atoms are intentionally confined to a single atomic plane in the host crystal, has been widely applied to the exploration of quantum effects in two-dimensional structures (where the doping profiles can be narrower than the de Broglie wavelength of electrons in the material), and has also led to important technological developments such as high mobility transistors, non-alloyed contacts, Schottky-gate transistors, and doping superlattice devices such as spatial light modulators and lasers.

The results of our calculations of the electronic structure of the clean and doped GaAs(110) cleaved surface, and associated theoretical X-STM images at varying bias voltages, have led to several interesting predictions, including: (1) Si does not behave as a conventional donor on the surface; (2) the electronic state associate with Si lies deep in the gap and is very localized on the surface; (3) at negative bias voltages, the signature of the Si atom has enhanced intensity at 3rd-nearest neighbor sites; and (4) for positive bias, the signature of Si would be that of a missing atom on the surface (!) The latter result is shown in figure 8. These predictions have recently been experimentally confirmed by Professor E. Weber's group at the University of California at Berkeley.

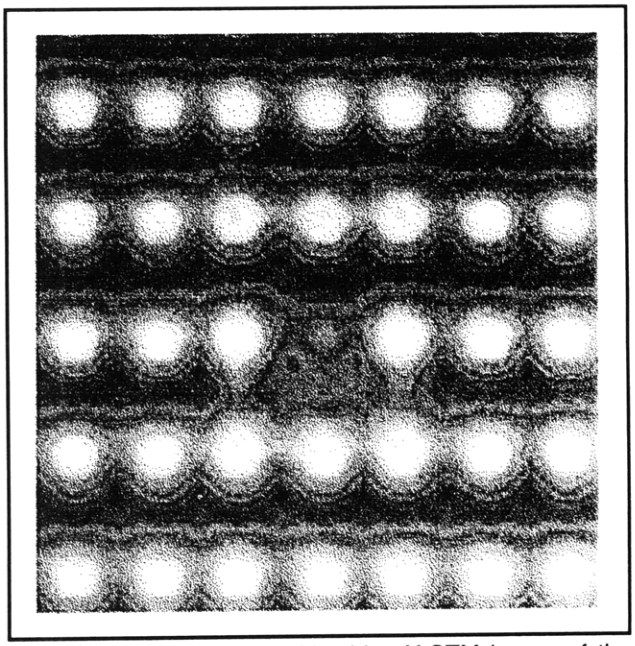

Figure 8. Theoretical positive-bias X-STM image of the GaAs (110) surface with a Si impurity. What appers to be a missing Ga atom is in fact the signature of the Si atom.

4.4 Publications

Arias, T., and J.D. Joannopoulos. "The View of Grain Boundaries and Segregation from the Computational Leading Edge." *Electrochem. Soc. Proc.*, 1993.

Brommer, K., B. Larson, M. Needels, and J.D. Joannopoulos. "Modeling Large Surface Reconstructions on the Connection Machine." *J. Appl. Phys.* 32: 1360 (1993).

Brommer, K., B. Larson, M. Needels, and J.D. Joannopoulos. "Implementation of the Car-Parrinello Algorithm for Ab-Initio Total Energy Calculations on a Massively Parallel Computer." *Computers in Phys.* 7(3): 350 (1993).

Cho, K., T. Arias, and J.D. Joannopoulos. "Wavelets in Electronic Structure Calculations." *Phys. Rev. Lett.* 71: 1808 (1993).

Cho, K., J.D. Joannopoulos, and L. Kleinman. "Constant Temperature Molecular Dynamics with Momentum Conservation." *Phys. Rev. E* 47: 3145 (1993).

Dal Pino, A., Jr., M. Galvan, T. Arias, and J.D. Joannopoulos. "Chemical Softness and Impurity Segregation at Grain Boundaries." *J. Chem. Phys.* 98: 1606 (1993).

Dal Pino, A., Jr., A. Rappe, and J.D. Joannopoulos. "Ab-Initio Investigation of Carbon Related Defects in Silicon." *Phys. Rev. B* 47: 12554 (1993).

Galvan, M., A. Dal Pino, Jr., J. Wang, and J.D. Joannopoulos. "Local Softness, STM and Surface Reactivity." *J. Phys. Chem. Lett.* 97: 783 (1993).

Galvan, M., A. Dal Pino, Jr., and J.D. Joannopoulos. "Hardness and Softness in the Ab-initio Study of Polyatomic Systems." *Phys. Rev. Lett.* 70: 21 (1993).

Meade, R., A. Rappe, K. Brommer, and J.D. Joannopoulos. "Accurate Theoretical Analysis of Photonic Band-Gap Materials." *Phys. Rev. B* 48: 8434 (1993).

Meade, R., A. Rappe, K. Brommer, and J.D. Joannopoulos. "The Nature of the Photonic Band Gap." *J. Opt. Soc. Am. B* 10: 328 (1993).

Robertson, W., G. Arjavalingam, R. Meade, K. Brommer, A. Rappe, and J.D. Joannopoulos. "Observation of Surface Photons on Periodic Dielectric Arrays." *Opt. Lett.* 18: 528 (1993).

Robertson, W., G. Arjavalingam, R. Meade, K. Brommer, A. Rappe, and J.D. Joannopoulos. "Measurement of the Photo Dispersion Relation in 2D Ordered Dielectric Arrays." *J. Opt. Soc. Am. B* 10: 322 (1993).

Wang, J., T. Arias, and J.D. Joannopoulos. "Dimer Vacancies and Dimer Vacancy Complexes on Si(100)." *Phys. Rev. B* 47: 10497 (1993).

Wang, J., T. Arias, J.D. Joannopoulos, G. Turner, and O. Alerhand. "STM Signatures and Chemical Identifications of the (110) Surface of d-doped GaAs." *Phys. Rev. B* 47: 10326 (1993).